Microstructural modification in Co/Cu giant-magnetoresistance multilayers

C. Christides,[a] S. Stavroyiannis, N. Boukos, A. Travlos, and D. Niarchos
Institute of Materials Science, NCSR ''DEMOKRITOS,'' 153 10 Agia Paraskevi, Attiki, Greece

(Received 21 July 1997; accepted for publication 22 December 1997)

Three different classes of $[\mathrm{Co}/1.1\ \mathrm{nm}/\mathrm{Cu}/2.1\ \mathrm{nm}]_{30}$ multilayers were grown by magnetron sputtering deposition. The effect of magnetostatic interactions on the giant-magnetoresistance (GMR) and magnetic properties are examined in relation to the induced changes in the film microstructure as it is varied by: (i) the substrate surface roughness and (ii) the effect of thermal isolation of the Si(100) substrate from the cooling plate during deposition. A remarkable variation in shape and magnitude of GMR, and in the magnetic (M-H) loops, is observed for the three classes of films. It is found that there are three characteristic features in every sample that vary systematically: (i) The $(\Delta R/R)_{\max}$ ratio. (ii) The magnetic field range where a GMR loop reaches its minimum value. (iii) The (M-H) loops that vary from the characteristic antiferromagnetic to a typical ferromagnetic loop shape. Two well-separated grain size distributions below and above 12 nm were found from transmission electron microscopy. The smaller grains are associated with the appearance of a considerable fraction of ferromagnetically coupled regions in the multilayer. © *1998 American Institute of Physics.* [S0021-8979(98)04107-3]

I. INTRODUCTION

The giant-magnetoresistance (GMR) effect is of interest for applications in magnetoresistive recording heads or sensors and has stimulated much of the activity in this field. GMR arises in a variety of magnetic systems including multilayers (MLs), spin valves, and granular materials.[1] The largest GMR ratios have been found in sputtered polycrystalline Co/Cu MLs and exceed 60% at room temperature (RT).[2] In Co/Cu MLs the ratio: $\mathrm{MR}_{\max}=(R_{\max}-R_s)/R_s$, with $R_{\max}$ and R_s the maximum and minimum resistance as a function of the applied magnetic field, H, respectively, is an oscillating function of Cu thickness (t_{Cu}) with three well defined maxima. These occur at $t_{\mathrm{Cu}}\approx 0.9$, 2, and 3 nm,[3] and correspond to antiferromagnetic (AF) coupling between neighboring Co layers. Although very large GMR values are obtained in Co/Cu and other Cu-based MLs at RT, the required saturation field (H_s) to reach R_s, is large. At the first AF peak (AF1) the H_s is $\approx$4 kOe for $t_{\mathrm{Co}}=1$ nm with a triangularly shaped $\Delta R/R$ vs H curve. The observed rapid decrease of interlayer coupling with increasing t_{Cu} makes it possible to obtain MR ratios of 30% at RT for $H_s\approx 200$ Oe at the second AF peak (AF2).[4] The field dependent sensitivity $S(H)=(1/R)(dR/dH)$ is another critical parameter that defines the change of resistance per unit field in these devices. It has a maximum value $S_{\max}\propto \mathrm{MR}_{\max}/H_s$, assuming that the $\Delta R/R$ vs H-applied curve has a peak that may be approximated by a triangle. However the GMR change per unit field is still low compared to thin films of permalloy and, most important, the shape of loops at AF2 is different from the triangularly shaped curves at the AF1 peak. Usually, apart from the AF1 peak, the $\Delta R/R$ vs H loops exhibit a double-peaked MR curve when the field H sweeps in opposite directions, and they exhibit a maximum resistance ($R_{\max}$) at fields corresponding to the $\pm H_c$, where H_c is the coercive field. Thus, large H_s fields and the existence of hysteresis in GMR curves manifest the major difficulties for direct application of Co/Cu MLs in magnetic sensors.

The range of the reported GMR ratios for t_{Cu} values at the AF1 and AF2 points,[2–6] in sputter grown Co/Cu MLs, indicates that microstructure features are responsible for the large differences observed in the $\Delta R/R_s$ vs H isothermal GMR curves. The properties of such magnetic MLs are sensitive to growth conditions, the substrate material, and the buffer layer, if any, between the substrate and multilayer.[5] Consequently, it is necessary to develop the appropriate microstructure in these MLs that will reduce both: (i) the interlayer AF coupling energy (J_{AF}), which would induce lower H_s, and (ii) hysteresis in the GMR curves, by appropriate modification of the magnetization reversal process of magnetic domains. In epitaxial grown wedges it is shown[7] that: (i) $J_{\mathrm{AF}}\approx M_s H_s t_{\mathrm{Co}}$, with M_s the Co layer saturation magnetization, and (ii) J_{AF} is independent of t_{Co} but varies as $1/t_{\mathrm{Cu}}^2$. The Ruderman–Kittel–Kasuya–Yosida (RKKY) oscillations through the spacer, whose period depends on Fermi surface parameters, are used to explain this behavior. Thus, when $H_s\approx J_{\mathrm{AF}}/M_s t_{\mathrm{Co}}$ as is the case for MLs grown with a high degree of perfection in their layer-by-layer stacking, it is observed that the H_s and H_c quantities go in opposite directions when J_{AF} is reduced. In this case the influence of hysteresis becomes larger due to the decrease of the ratio of AF coupling to magnetic anisotropy energy: $J_{\mathrm{AF}}/K_A t_{\mathrm{Co}}$, with K_A the intrinsic magnetic anisotropy energy. However, magnetostatic effects arising from roughness in the Co/Cu interfaces favor interlayer ferromagnetic (FM) coupling if the magnetization is lying in the film plane.[8] These magnetic dipolar interactions modify the intrinsic effect of indirect exchange coupling that tends to oscillate as a function of t_{Cu} between FM and AF coupling. As a result, a considerable deviation from the antiparallel (180°) alignment of magnetic

[a]Electronic mail: christos@cyclades.nrcps.ariadne-t.gr, fax:+301-6519430.

moments in adjacent magnetic layers has been observed,[1] showing that the condition $J_{AF} \approx M_s H_s t_{Co}$ is not adequate to describe the observed variation of J_{AF}. This work has been initiated from the following two observations regarding the H_s and H_c variations:

(i) In a phenomenological expression, the total exchange interlayer coupling energy[9] and indirectly the MR ratio can be written as an even function of $m = M/M_s$ ratio:[1]

$$\Delta R/R = \mathbf{a} - \mathbf{b}m^2 - \mathbf{c}m^4 \quad (1)$$

for weakly coupled polycrystalline MLs in analogy to granular films. The quadratic term expresses the bilinear (180°) indirect coupling with $\mathbf{b} \propto \mathbf{A}_{12}$, where $\mathbf{A}_{12}$ is the AF exchange strength factor, and the biquadratic term expresses the 90° indirect coupling with $\mathbf{c} \propto \mathbf{B}_{12}$, where $\mathbf{B}_{12}$ is the biquadratic coupling strength factor. The correlation between the 90° coupling and MR oscillation as a function of t_{Cu} in Co/Cu MLs has been used[6] to explain why GMR in MLs with imperfect interfaces may result from 90° orientation of domains within adjacent Co layers. This correlation is important because it allows H_s to be minimized without canceling the GMR effect.

(ii) Nuclear magnetic resonance (NMR) measurements[10] show that the interface roughness in Co/Cu MLs depends significantly on the t_{Co}, and t_{Cu}. In addition, the coupling parameter depends not only on the spacer thickness but also on the thickness of the magnetic layers and on the grain size.[10] A systematic study of the t_{Co} influence on the GMR ratio, H_s and H_c at the AF1[11(a)] and AF2[11(b),(c)] peaks of Co/Cu MLs shows that reduced hysteresis and H_s in GMR curves can be obtained at the AF2 peak. This can be achieved by either forming MLs[11(b)] with very thin Co layers ($t_{Co} \approx 0.2-0.3$ nm) or with successive Co layers $t_{Co} \approx 1.5$ nm, alternated with $t_{Co} \approx 0.3$ nm layers[11(c)] in the superlattice stacking: Co/Cu/Co/../. Also ^{59}Co NMR experiments[12] at the AF2 peak as a function of t_{Co} indicate that the Co/Cu interfaces transform to discontinuous Co layers for $t_{Co} < 1$ nm. This property may be related to the observed disappearance of magnetoresistive hysteresis.[11(b)] Thus, appropriate modulations of the Co layer morphology may provide a way to alter the GMR properties in this system. Early studies[13] of the influence of substrate surface irregularities on the coercivity of permalloy thin films have also provided evidence that these may systematically alter H_s.

In the present study, as deposited Co/Cu MLs grown by magnetron sputtering on Si(100) substrates are examined with x-ray diffraction (XRD), transmission electron microscopy (TEM), MR, and magnetic hysteresis loop measurements. The purpose is to investigate the effect of magnetostatic interactions on the GMR and magnetic properties as a function of the changes induced in the film microstructure by varying: (i) the substrate surface roughness, and (ii) the thermal contact of the Si(100) substrate with the cooling plate during deposition.

II. EXPERIMENTAL DETAILS

Metallic disks of 99.99% pure elements with diameter 5 cm, were used as target materials in a high vacuum Edwards E360A sputtering system with a cluster of ATOM-TECH 320-SE planar magnetron sputter sources. The substrates were cut before deposition to a size of 12×4 mm^2. All samples were deposited in a cryogenically pumped chamber with a base pressure of 6×10^{-7} Torr under an Ar (99.999% pure) pressure of 3 mTorr. An rf magnetron gun operating at 30 W with a deposition rate of 0.09 nm/s was used for Co, and dc sputtering at 5 W for Cu, resulting in a rate of 0.1 nm/s. The thickness determination of the various layers is based on the deposition time assuming constant deposition rates. The thickness of MLs has been measured with low-angle XRD. XRD spectra were collected with a SIEMENS D500 powder diffractometer in $\theta-2\theta$ scans, using Cu K_α radiation at ambient temperature.

TEM specimens were prepared in planar and cross-section forms. The planar samples were prepared by mechanical polishing, dimpling, and final thinning by Ar^+ ion milling at 6 kV with the aid of a liquid nitrogen stage. The cross-section specimens were prepared by the same procedure, with a difference only in the final stage of ion milling where the accelerating voltage was reduced to 4 kV in order to minimize irradiation damage to the samples. TEM examination was performed with a Philips CM20 TEM operating at 200 kV.

Magnetic hysteresis loops were measured with a Quantum Design MPMSR2 superconducting quantum interference device (SQUID) magnetometer. MR measurements were performed in this SQUID with the four-point-probe method, using a dc current of 10 mA. All measurements were performed at 290 K by first applying the maximum positive field H parallel to film plane and then completing the loop.

The peak-to-peak surface roughness of the substrates has been estimated using the multi-mode atomic force microscope MMAFM-2/383 (AFM), using the Nanoscope III SPM from Digital Instruments. Two qualities of substrate surfaces can be distinguished from the AFM measurements: (1) atomically perfect surfaces with an observed peak-to-peak roughness of less than 4 nm and (2) optically perfect surfaces with peak-to-peak roughness ranging between 4 and 15 nm. The Si(100) surface roughness, and the existence or not of thermal contact between the substrate and the cooling plate during deposition, define the three classes of Co/Cu films prepared. Thus, samples A, B, and C denote MLs grown on substrates with (i) atomically perfect surfaces in thermal contact with the cooling plate, (ii) atomically perfect surfaces isolated thermally from the cooling plate during deposition, and (iii) optically perfect surfaces thermally isolated from the cooling plate during deposition, respectively.

III. EXPERIMENTAL RESULTS

A. Structural characterization

1. XRD

The XRD spectra are characterized by an intense fcc (111) Co(Cu) peak and a weak (200) fcc peak, indicating that the MLs have strong (111) in-plane texture. A fit of these Bragg peaks with a Lorentzian peak shape function gives the peak position, the full width at half maximum (FWHM) β in 2θ degrees, and the ratio of the integrated intensities

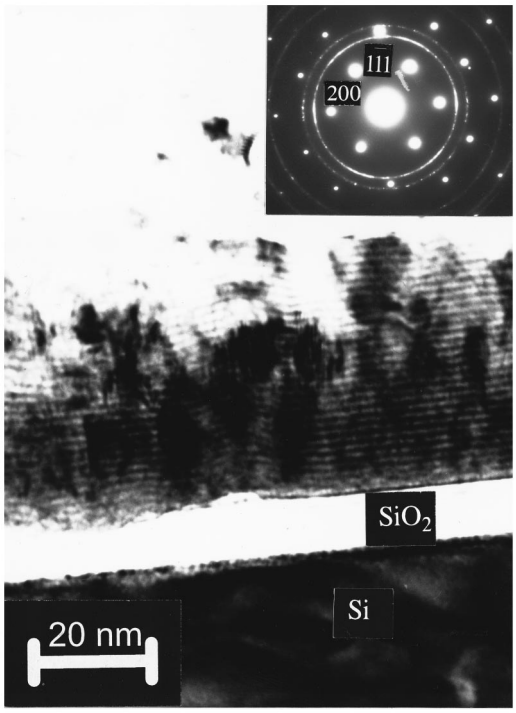

FIG. 1. A typical cross-section TEM micrograph for sample C. Magnification 200 000 times. The corresponding SAED images are shown on top of the micrograph, where the Si[200] spots can easily be seen. The inner diffraction ring of the multilayer corresponds to (111) fcc atomic planes and expresses the degree of preferential orientation along the Si[200] direction.

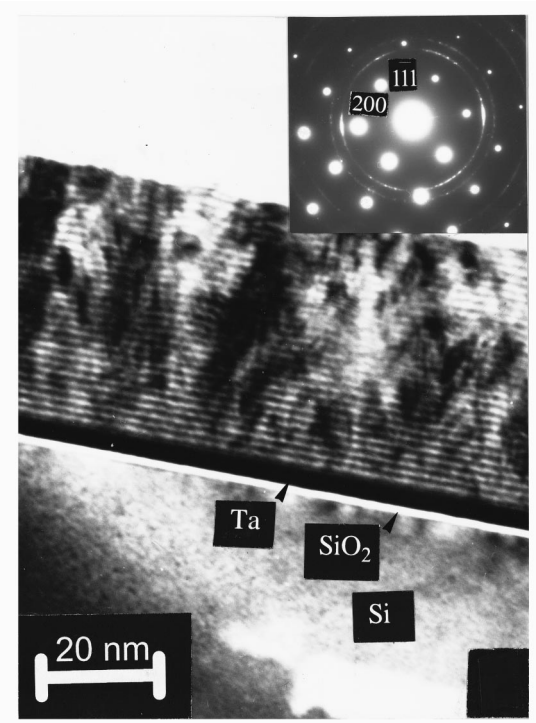

FIG. 2. A typical cross-section TEM micrograph for sample B. Magnification 200 000 times. The corresponding SAED images are shown on top of the micrograph, where the Si[200] spots can easily be seen. The inner diffraction ring of the multilayer corresponds to (111) fcc atomic planes and expresses the degree of preferential orientation along the Si[200] direction.

I_{111}/I_{200}. For class A films the obtained parameter: $\beta_{111}(\mathrm{A})=0.6°$, from the Scherrer equation,[6] corresponds to an average grain size of 15 nm which is close to the size observed with TEM. However, for class C and B MLs the use of the Scherrer formula predicts average grain sizes that are far from those observed in the TEM because of the peculiar distribution of the grain sizes which is discussed in the next subsection.

2. TEM

TEM images were obtained from Si(100)/{buffer/$[\mathrm{Co/1\ nm/Cu/2.1\ nm}]_{30}$ MLs which were grown under the different conditions (A, B, C) already described. The sample A film is grown on a 500 nm SiO_2 buffer layer with an atomically perfect surface and the Si(100) substrate in thermal contact with the cooling plate. Sample B is grown on a 10 nm Ta buffer with an atomically perfect surface and the Si(100) substrate thermally isolated from the cooling plate. Sample C is grown on native SiO_2 with an optically perfect surface and the Si(100) substrate thermally isolated from the cooling plate.

Typical bright field micrographs of the sample cross sections can be seen in Figs. 1–3. The Si substrate is oriented in the [011] zone axis, so that the Si/multilayer interface is parallel to the electron beam. The following characteristics can be seen in the micrograph of Fig. 1 that correspond to sample C. There are areas where the Si/multilayer interface has a roughness about 5 nm while the native SiO_2 layer (white strip) is about 10 nm thick. On top of the ~5 nm dip area the Co/Cu MLs exhibit irregularities that induce lateral and transverse uncorrelated roughness (left to middle part of Fig. 1) while over the flat part of the substrate the layer stacking follows the shape of the underlying interface (right part of Fig. 1). Lower magnification micrographs reveal areas where the Si/multilayer interface has a roughness about 15 nm where the Co/Cu overlayers are wavy, following the shape of the underlying interface while towards the top of the MLs the Co/Cu layers are bedded or interrupted in several areas. The overall quality of the C multilayer is inferior to the B film grown on Ta buffer layer (Fig. 2). The successive layers of native SiO_2 (~2 nm white strip), Ta buffer (~10 nm black strip) and Co/Cu multilayer (t_{Co}~1 and t_{Cu}~2 nm) can be clearly seen for sample B in Fig. 2. The Co/Cu layers are smooth and uniform in thickness, especially near the buffer interface. Towards the top of the multilayer the quality progressively becomes worse and the peak to valley roughness is ~1 nm. The quality of sample A is better again as can be seen in Fig. 3, where the Co/Cu layers look smooth and well separated from top to bottom of the columnar grains although the image fades near the 500 nm amorphous SiO_2 buffer layer.

The elongated structures—normal to the interface—that penetrate the superlattice in these MLs are crystallites, indicating the existence of columnar growth. In order to determine the preferred orientation of the columnar structures, selected-area electron diffraction (SAED) patterns of the multilayers were obtained (insets in Figs. 1, 2, 3). It is worth noting that the first six spots from the Si substrate around the central bright spot do not form a hexagon but are separated

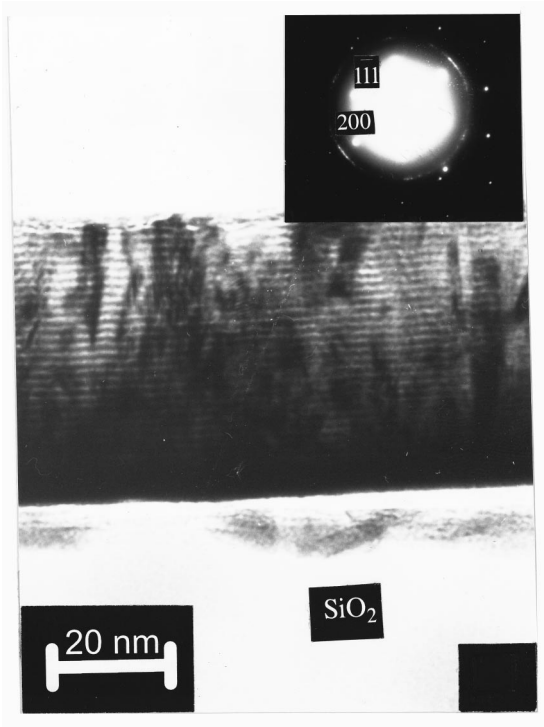

FIG. 3. A typical cross-section TEM micrograph for sample A. Magnification 200 000 times. The corresponding SAED images are shown on top of the micrograph, where the Si[200] spots can not be easily seen due to diffuse scattering from the 500 nm of SiO_2 buffer layer. The diffraction ring of the multilayer corresponds to (111) fcc atomic planes and expresses the degree of preferential orientation along the Si[200] direction.

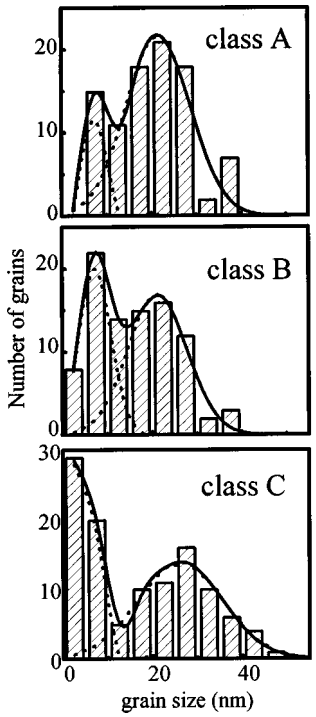

FIG. 4. The grain size distributions obtained from planar bright field TEM micrographs in samples A (top), B (middle), and C (bottom). The solid line is a fit of the total grain size distribution with two Gaussian line shapes and the dashed line shows the Gaussian components.

in a rectangularlike shape with spots indexed to the [110] direction and to a line with spots corresponding to [200]. For sample C the SAED pattern (inset of Fig. 1) shows almost uniform bright rings that are indexed to (111)-inner, (200), (220) and (311) Co/Cu fcc planes, indicating a practically zero degree of preferred orientation. But for sample B the nonuniform intensity of the (111) Co/Cu ring, which is clearly brighter along the (200) Si substrate spots (Fig. 2), is evidence that the (111) crystallites grow with preferential orientation with respect to the Si substrate. Since the MLs are grown on Si(100), the part of the Co/Cu(111) ring that is parallel to the Si [200] direction corresponds to Co/Cu(111) planes parallel to the Si(100)/multilayer interface. In sample A the intensity of the (111) Co/Cu ring along the [200] Si direction is higher than any other (Fig. 3). Thus, a comparison of SAED patterns reveals a higher degree of preferred orientation of the MLs (111) texture relative to the substrate [200] direction in samples A and B relative to C.

The dark field images, obtained by using the part of (111) Co/Cu rings that are parallel to [200] Si direction, show that in sample A there are large columnar structures (crystallites) with similar longitudinal dimensions. In sample B these crystallites form columns extending throughout the film thickness, while in sample C there is a considerable fraction of smaller intervening structures with arbitrary shape. The heights of the columnar crystallites extend from 60 to 90 nm for sample A whereas in samples B and C they display a larger dispersion, between 30 and 90 nm. Furthermore, the total volume of the observed dark features in these micrographs indicate that the corresponding fraction of (111) Co/Cu crystallites exhibiting a preferred orientation relative to [200] Si substrate direction for A and B MLs is higher than in C MLs. However, the dark field images of $(\bar{1}11)$ Co/Cu crystallites oriented parallel to $(\bar{1}11)$ and (111) Si planes show that samples A, B, and C do not form coherent columnar structures along these directions in any of these MLs. This is an indication that Co/Cu (111) textured crystallites grow exclusively with a preferred orientation parallel to [200] Si substrate direction.

In order to obtain a complete picture of texture and grain size, it was necessary to examine the MLs in a direction at right angles to the one investigated above. Thus planar specimens were examined oriented in the [100] Si zone axis. The SAED patterns did not show any sign of Co/Cu(111) preferential orientation in any of the three MLs. Consequently, texturing occurs only for these (111) Cu/Co crystallites having a zone axis parallel to the Si/[Co/Cu] interface. The grain size distribution obtained from the planar images, with 80.000 times magnification, is plotted in Fig. 4 for samples A, B, and C. As a first approximation, two Gaussian peaks can produce a satisfactory fit of the grain size distribution. It is obvious that there are two well separated populations of grain sizes, below and above ~12 nm for sample C. The fraction of small grains decreases in sample B, and finally the population of larger crystallites becomes dominant for sample A. It is discussed below how these differences in grain size distributions are expected to influence the magnetic and magnetotransport properties of the three classes of Co/Cu MLs.

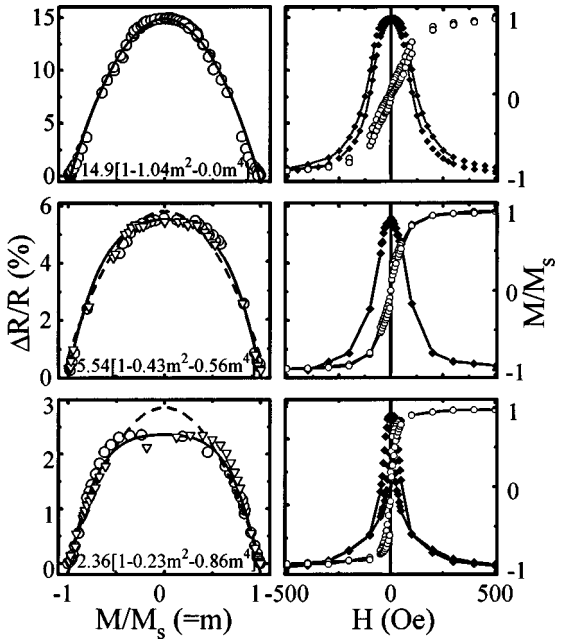

FIG. 5. (Right side) The dependence of GMR ratio $\Delta R/R$ (left axis) and reduced magnetization M/M_s hysteresis loops (right axis) vs H is shown for samples A (top), B (middle), and C (bottom). (Left side) The $\Delta R/R$ vs M/M_s data sets, obtained for the same H values, from the corresponding right side plots are shown. The triangles and circles indicate decreasing and increasing magnetic field, respectively, while the dashed and solid lines correspond to fits without and with nonzero biquadratic terms from Eq. (1). The equations that produce the best fitting curves are also displayed.

B. GMR and magnetic measurements

1. Comparison of samples A, B, and C

Samples A and B are grown on substrates with surface roughness less than 4 nm, either in good thermal contact or thermally isolated from the cooling plate during deposition, respectively. Although different buffer layers were used to control the substrate surface roughness, it is demonstrated in Sec. B 2 below that the used buffers do not affect the GMR properties beyond their surface roughness. In sample C both substrate thermal isolation and enhanced surface roughness (>4 nm) are introduced. In Fig. 5 (right column) the dependence of GMR (left axis) and reduced magnetization (right axis) hysteresis loops for sample A (top), sample B (middle), and sample C (bottom) is shown. All the measurements are performed with H parallel to the film plane at right angles to current flow direction and are the same specimens that were examined with TEM. There is a remarkable variation in shape and magnitude of GMR, and in the magnetic (M-H) loops also, for the three films. There are three characteristic features that vary systematically as we progress from sample A to C:

(i) There is a decrease of the $(\Delta R/R)_{\max}$ ratio.
(ii) There is a narrowing of the magnetic field range where a GMR loop reaches its minimum value.
(iii) A change occurs in the (M-H) loops from the characteristic AF to a FM loop shape.

On the left side of Fig. 5 the variation of $\Delta R/R$ versus the reduced magnetization M/M_s is plotted, for the field values H obtained from the corresponding hysteresis loops displayed on the right side of Fig. 5. A fit with Eq. 1 has been performed including either the quadratic and biquadratic terms (solid line) or the quadratic term only (dashed line). The equations that give the best fit are also shown. The variation from pure quadratic to a strongly biquadratic influence is evident from the shape changes in the curves of A to C films. The $M/M_s=m$ variable corresponds to the variation of $\cos 2\theta$ as a function of H, where 2θ is the average angle between the magnetic moments in neighboring Co layers. If the observed effect was due only to the exchange energy $E_{\rm ex}$ that couples two successive FM layers through the Cu spacer, then the total energy would be written:[14]

$$E=E_{\rm ex}(\theta)-HM_s t_{\rm Co}\cos\theta \quad \text{with}$$

$$E_{\rm ex}(\theta)=A_{12}M_s^2(1-\cos 2\theta)+B_{12}M_s^2(1\text{-}\cos 4\theta). \qquad (2)$$

Minimization of the total energy in Eq. (2) leads to an implicit variation of M vs H. A fit of the observed (M-H) loops in NiFe/Ag MLs[14] to this expression gave values for the bilinear and biquadratic coupling terms in Eq. (1) that are almost independent of the NiFe thickness. However the same expression does not fit any of the observed (M-H) loops in our Co/Cu MLs indicating that either the magnetic anisotropy term or the fraction of FM coupled layers has a dominant effect. Since the $t_{\rm Co}$ is the same for these samples then the intrinsic magnetic anisotropy should not be different. Consequently, strain, dipole field interactions, and other layer morphology effects can be associated with the observed changes in magnetic properties. In these samples our planar TEM images (Fig. 4) show that there is a bimodal distribution of grain sizes with a considerable fraction of grains of average size less than 10 nm increasing from samples A to C. The increasing fraction of smaller grains creates a larger number of grain boundaries where magnetostatic effects will favor the formation of magnetic domains with a broad distribution of local magnetic vector orientations within a Co layer. In addition, the fraction of Co/Cu crystallites that exhibit a preferred orientation of their (111) planes along the Si [200] direction is found to decrease from samples A to C. This energetically favors a progressive misalignment of magnetic moments for the three different specimens. These two changes in microstructure may alter the interlayer magnetic configuration from AF in sample A to FM in sample C. Thus, for these measurements the coefficients **b** and **c** in Eq. (1) are rather complicated functions of the exchange strength factors because FM exchange coupling does not appear as a linear superposition in the AF coupling terms. The topological magnetostatic effect resulting from Co/Cu interface roughness, which may create dipole fields favoring FM alignment in Co layers, competes with the oscillatory (RKKY) indirect exchange coupling between adjacent magnetic layers. In this way both interactions can control the observed magnetic and magnetotransport properties. According to Figs. 4 and 5 a 30% fraction of grain sizes with average diameter less than about 10 nm may be related to the appearance of extended FM interlayer coupling that may indirectly affect the configuration of magnetic moments in the Co layers of the larger crystallites.

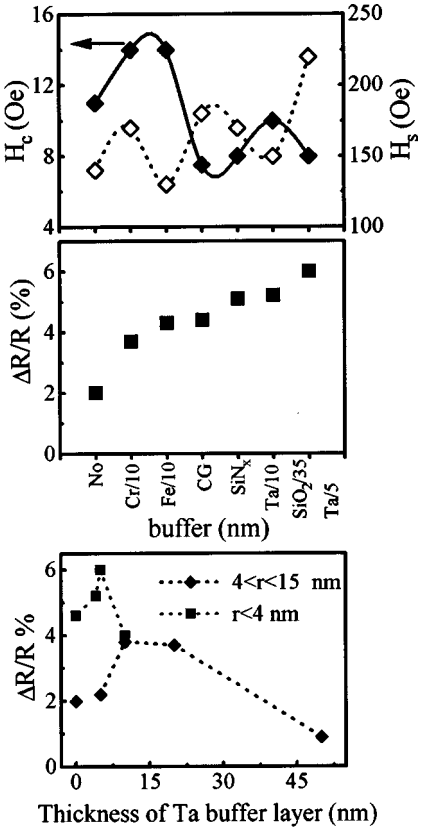

FIG. 6. The influence of substrate surface peak-to-peak roughness r on the GMR effect (bottom) is demonstrated for samples B (square) and C (diamond): Si(100)/{Ta/t_{Ta}/[Co/1 nm/Cu/2.1 nm]$_{30}$}. The upper part shows the dependence of the GMR ratio ($\Delta R/R$ middle), and the variation of the obtained H_c, H_s parameters (top), as a function of the buffer material in Si(100)/{buffer/[Co/1 nm/Cu/2.1 nm]$_{30}$} multilayers grown on thermally isolated substrates. The adjacent numbers to the buffer material indicate their layer thickness in nm.

2. Influence of buffer layers and Si(100) surface roughness on samples B and C

The research on the effect of buffer layers[3] has shown that the optimum buffer to produce the maximum GMR ratio is a layer of Fe about 5 nm thick and our results in the class A films coincide with this finding. However, the switching and especially the coercive field resulting from this buffer are high enough to exclude such samples from applications. In the following, the buffer layer effect will be demonstrated for Co/Cu MLs grown on substrates thermally isolated from the cooling plate.

First, in order to investigate the influence of buffer thickness on the GMR effect, Ta was grown directly on Si(100) substrates covered with native SiO_2. The peak-to-peak substrate surface roughness (r) has been classified from AFM measurements in two groups with $r<4$ nm and $4<r<15$ nm that were used for class B and C deposition conditions, respectively. In Fig. 6 (bottom) the dependence of $(\Delta R/R)_{max}$ upon the Ta buffer thickness is shown for Si(100)/{Ta/t_{Ta}/[Co/1 nm/Cu/2.1 nm]$_{30}$} MLs grown on substrates with $r<4$ nm (square symbols—class B) and $4<r<15$ nm (diamond symbols—class C). For class B films a maximum occurs at $t_{Ta}\approx 5$ nm and for samples C at $t_{Ta}\approx 12$ nm. These values are comparable to the substrate surface roughness r, indicating that Ta is wetting the substrate surface in a way that reduces the initial roughness. For large t_{Ta} (>10 nm) there is a common reduction of the GMR effect probably due to shunting of the current through the buffer.

Second, the influence of several buffers in the GMR properties for MLs grown on thermally isolated Si(100) substrates is examined. The dependence of $(\Delta R/R)_{max}$, H_c, and H_s parameters on the buffer material for Si(100)/{buffer/[Co/1 nm/Cu/2.1 nm]$_{30}$} MLs is shown in Fig. 6 (top). Note that the surface Si(100) roughness is less than 4 nm peak-to-peak, and that the $\Delta R/R\sim 2\%$ value observed for sample C ($r>4$ nm) without buffer, labeled in Fig. 6 as (No), is included for comparison.

The buffer layer thicknesses displayed in Fig. 6 (middle) are those that give the best GMR ratios for each type of buffer. A film grown directly on Corning glass (CG) is also included for comparison. Note that no structural changes have been detected, from XRD measurements, as a consequence of changes in the buffer or the substrate material. The variations of the GMR loop parameters in Fig. 6 (top) indicate that the films with 10 nm Ta buffer layer or with a SiN_x surface layer are those that combine the highest GMR ratio with relatively low H_c and H_s values.

IV. SUMMARY AND CONCLUSIONS

A comparative investigation of GMR and magnetic properties in Co/Cu MLs, at the AF2 peak, with three different microstructures, is presented for the first time. A quantitative estimate of the substrate surface roughness and the effect of the buffer layer in the modification of this roughness is given. The development of a specific microstructure, in terms of grain size and degree of layer texturing leading to macroscopic GMR parameters appropriate for use in active magnetic sensors, is achieved. In summary, there are some major results relating microstructure with optimum sensing conditions of GMR curves in sputtered Co/Cu MLs:

(i) The substrate surface roughness, with or without buffer layer, should be less than 4 nm in order to have columnar growth of crystallites with a distribution of grain sizes ~20 nm. A substrate starting roughness larger than 4 nm requires a thicker Ta buffer layer, more than 10 nm, to reduce surface roughness but leads to a depression of the GMR effect probably due to increased current shunting. Alternatively, a SiN_x buffer layer produces equivalent results in the GMR properties with the Ta buffer without current shunting.

(ii) The growth of structures with average sizes less than 10 nm, with a volume fraction of ~30%, seems to increase the fraction of FM areas. A substrate or buffer induced peak-to-peak surface roughness less than 4 nm, and thermal isolation of the substrate from the cooling plate produces an appropriate microstructure which exhibits GMR properties suitable for sensor applications.

(iii) The SAED planar TEM images show that at right angles relative to the Si surface there is not any preferred orientation of the (111) Co/Cu planes for all the examined MLs. However, the SAED cross-section patterns show that there is some degree of preferred orientation in the (111) Co/Cu planes relative to the Si [200] substrate direction for

samples A and B only. Thus, the degree of preferred orientation of Co/Cu(111) planes relative to Si [200] substrate direction is found to decrease going from sample A to C, being zero for sample C. In addition, a larger fraction of grains with sizes less than 10 nm appears progressively from sample A to C. The results shown in Fig. 4 reveal that for sample A the fraction of columnar grains with sizes more than 15 nm is about 90%, for sample B it is ~70%, and in sample C is less than 50%.

(iv) To date, two different approaches have been reported in Co/Cu based structures that target low H_c and H_s values: Either by forming MLs with $t_{Co} \approx 1.5$ nm alternated with $t_{Co} \approx 0.3$ nm layers[11(c)] in the superlattice stacking: Co/Cu/Co/../, or using spin-valve systems,[15,16] where a surfactant layer of In or Pb or Au is introduced to control the long-wavelength (waviness) interface roughness. Here, a third way has been demonstrated to systematically control the magnetostatic effects in Co/Cu MLs by selecting the surface substrate roughness and by using thermal isolation of the Si(100) substrate during magnetron sputtering with slow deposition rates of the constituents.

ACKNOWLEDGMENT

This work has been supported by the EKBAN-280 project of the General Secretariat for Research and Technology of the Development Ministry in Greece.

[1] S. S. P. Parkin, in *Ultrathin Magnetic Structures II*, edited by B. Heinrich and J. A. C. Bland (Springer, (Berlin, 1994), Chap. 2.
[2] S. S. P. Parkin, Z. G. Li, and D. J. Smith, Appl. Phys. Lett. **58**, 2710 (1991).
[3] S. S. P. Parkin, R. Bhadra, and K. P. Roche, Phys. Rev. Lett. **66**, 2152 (1991).
[4] S. S. P. Parkin, Mater. Res. Soc. Symp. Proc. **231**, 211 (1992).
[5] A. R. Modak, D. J. Smith, and S. S. P. Parkin, Phys. Rev. B **50**, 4232 (1994).
[6] Z. J. Yang and M. R. Scheinfein, Phys. Rev. B **52**, 4263 (1995); Appl. Phys. Lett. **66**, 236 (1995).
[7] Z. Q. Qiu, J. Pearson, and S. D. Bader, Phys. Rev. B **46**, 8659 (1992).
[8] L. Neel, Comp. Rend. Acad. Sci. (France) **255**, 1545 (1962); **255**, 1676 (1962).
[9] M. Ruhring, R. Schafer, A. Hubert, R. Mostler, J. A. Wolf, S. Demokritov, and P. Grunberg, Phys. Status Solidi A **125**, 635 (1991).
[10] C. Meny, P. Panissod, and R. Loloee, Phys. Rev. B **45**, 12269 (1992).
[11] (a) D. J. Kubinski and H. Holloway, J. Appl. Phys. **79**, 7395 (1996); (b) **79**, 1661 (1996); C. H. Holloway and D. J. Kubinski, *ibid.* **79**, 7090 (1996).
[12] E. Jedryka, M. Wojcik, S. Nadolski, D. J. Kubinski, and H. Holloway, J. Magn. Magn. Mater. **165**, 292 (1997).
[13] A. G. Lesnik, G. I. Levin, and S. N. Kaverina, Acad. Sci. USSR, Phys. Ser. **29**, 594 (1965).
[14] C. Cowache, B. Dienny, A. Chamberod, D. Benizri, F. Berthet, S. Auffret, L. Giacomoni, and S. Nossov, Phys. Rev. B **53**, 15027 (1996).
[15] W. F. Egelhoff, Jr., P. J. Chen, C. J. Powell, M. D. Stiles, and R. D. McMichael, J. Appl. Phys. **79**, 2491 (1996).
[16] W. F. Egelhoff, Jr., P. J. Chen, C. J. Powell, M. D. Stiles, R. D. McMichael, C.-L. Lin, J. M. Sinertsen, J. H. Judy, K. Takano, and A. E. Berkowitz, J. Appl. Phys. **80**, 5183 (1996).